Available online at www.sciencedirect.com

ScienceDirect

Procedia Engineering 10 (2011) 3417–3422

Engineering Procedia

ICM11

Tensile Deformation and Fracture Properties of Irradiated SA533B Steel

Jin Weon Kim[a]*, Thak Snag Byun[b]

[a] *Department of Nuclear Engineering, Chosun University, Republic of Korea*
[b] *Oak Ridge National Laboratory, Material Science and Technology Division, United State*

Abstract

Irradiation effects on the stable and unstable deformation behavior and fracture properties of SA533B steel have been studied in detail based on the equivalent true stress versus true strain curves. An iterative finite element simulation technique was used to obtain the equivalent true stress-true strain curves from experimental load-displacement data. The results showed the localized necking occurs without diffuse necking for high dose irradiated cases that showed negligible uniform ductility in engineering stress-strain curves. Slope of true stress-strain curves was still positive during the unstable necking deformation regardless of irradiation dose level, and the slope considerably varied with necking mode change rather than with irradiation dose level. The equivalent fracture stress decreased with increase in dose level up to 0.1dpa and slightly increased above dose level. The equivalent fracture strain decreased with increasing dose level up to 0.1dpa and then decreased at lower rate, but it was still high after high dose irradiation exposure even if uniform ductility was almost zero. These dose dependences of tensile fracture stress and fracture strain are related with the fact that density of irradiation induced defects increases with increasing dose and is saturated at dose around 0.05dpa.

Selection and peer-review under responsibility of ICM11

Keywords: Irradiation effet; SA533B steel; Deformation behavior; Frcature; Finite element simulation

1. Introduction

One of the major aging mechanisms of nuclear components is degradation of material properties caused by irradiation, so it is important to understand the characteristics of irradiated materials for structural design and life time evaluation of nuclear components. A number of studies have been conducted to clarify the change in the mechanical properties of materials under intense radiation environment [1-4]. The results showed that the strength, ductility, and strain hardening capacity were significantly changed by irradiation. In particular, the irradiation hardening was often accompanied by changes in the stress-strain curve along with the appearance of yield drop and by a significant reduction in strain hardening capacity [4-5]. However, most of these radiation-induced changes were

* Corresponding author. Tel.: +82-62-230-7109; fax:. +82-62-232-9218
E-mail address: jwkim@chosun.ac.kr

Selection and peer-review under responsibility of ICM11 doi:10.1016/j.proeng.2011.04.563

observed for the uniform deformation regime only based on the engineering stress (σ_E)- engineering strain (ε_E) curves, and consequently the radiation effect on the unstable deformation has been often ignored although in most cases its range is larger than that for uniform deformation. To understand the radiation effect on deformation and fracture characteristics of materials in detail, therefore, it is necessary to produce full true stress-true strain data covering yielding, uniform deformation, unstable deformation, and final failure.

It was shown that the analysis of true stress (σ_T)-true strain (ε_T) data can suggest new descriptions for irradiation effect on strength and ductility of materials, and it also can evaluate irradiation effect on plastic instability and fracture properties [5-7]. Byun [5,6] investigated irradiation effects on the fracture stress (σ_F), fracture strain (ε_F), and strain hardening rate from the tensile data for various materials using liner strain hardening approximation. However, it was based on the nominal true stress and true strain relationship instead of equivalent true stress and true strain relationship that represents more general stress and strain response of a material and is nearly independent of specimen geometry. Recently, our previous study developed a procedure for determining full equivalent true stress-true strain curve including unstable necking deformation in tensile data and investigated the irradiation effect on the deformation behavior and fracture properties from tensile data for irradiated austenitic stainless steels based on equivalent true stress and true strain relationship [8]. It is known that FE simulation technique can accurately evaluate equivalent true stress-true strain curve from the tensile data given by flat specimen as well as round bar specimen [98].

The objective of this study is to investigate the irradiation effects on deformation behavior and fracture characteristic of irradiated SA533B steel from tensile data. This study determined full equivalent true stress-true strain curves including unstable necking deformation from tensile data for SA533B steel irradiated to various doses using FE simulation technique. The strain hardening rate and tensile fracture properties, equivalent fracture stress and fracture strain, were analyzed based on the equivalent true stress-true strain curves, and the dose dependence of these properties for SA533B steel was investigated.

2. Tensile Data

Tensile data for irradiated SA533B steel obtained from earlier study [4] were analyzed in the present study using iterative FE simulation technique. SA533B steel is a low alloy steel commonly used as reactor pressure vessel of a commercial light water reactor. The material was irradiated to five levels of neutron dose, 0.0, 0.001, 0.01, 0.1, and 0.89, and tested at ambient temperature. Irradiation was conducted at the hydraulic tube facility of the high flux isotope reactor (HFIR) at the Oak Ridge National Laboratory. In the HFIR irradiation facility, irradiation temperature was estimated to be in the range of 60-100^{o}C. Tables 1 and 2 summarize the chemical composition and thermo-mechanical treatment of the test material and the irradiation and test conditions, respectively.

Table 1 Materials and heat-treatment [9]

Material	Chemical composition	Heat treatment
SA533B	Fe-0.22C-0.25Si-1.48Mn-0.52Mo-0.68Ni-0.018S-0.012P	Annealed at 880^{o}C for 4h and air cooled, tempered at 660^{o}C for 4h, reheated at 610^{o}C for 20h.

Table 2 Irradiation and test conditions [9]

Material	Irradiation facility	Dose range (dpa)	Irradiation temperature (^{o}C)	Test temperature (^{o}C)	Specimen type
SA533B	HFIR	0-0.89	60-100	20	BES/NERI

Small-sized flat specimen (BES/NERI type), whose gage section dimension is 8mm×1.5mm×0.25mm, was employed for tensile tests. All tests were conducted in the screw-driven machine at quasi-static nominal strain rate of about $10^{-3}s^{-1}$. Figure 1 presents engineering stress-engineering strain curves of irradiated SA533B steel analyzed in the present study. The figure shows that the σ_E- ε_E curves are considerably changed by irradiation: increase in strength and decrease in elongation. In particular, the σ_E- ε_E curves irradiated to above 0.1dpa show negligible uniform plastic strains and a pseudo-yield drop followed by continuous softening to failure. This shows that the deformation behavior and ductility of SA533B steel is strongly affected by radiation exposure.

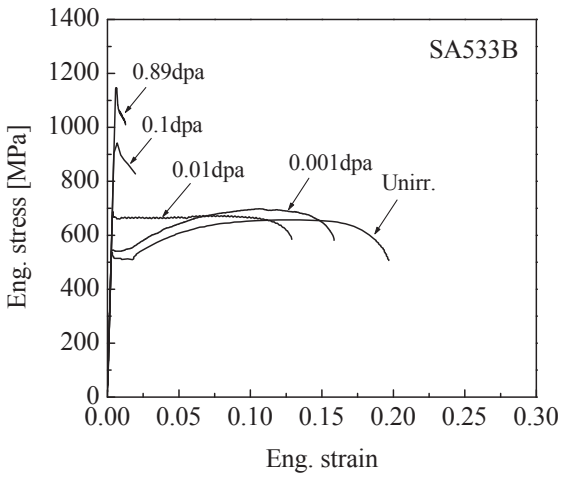

Fig. 1 Engineering stress-engineering stress curves

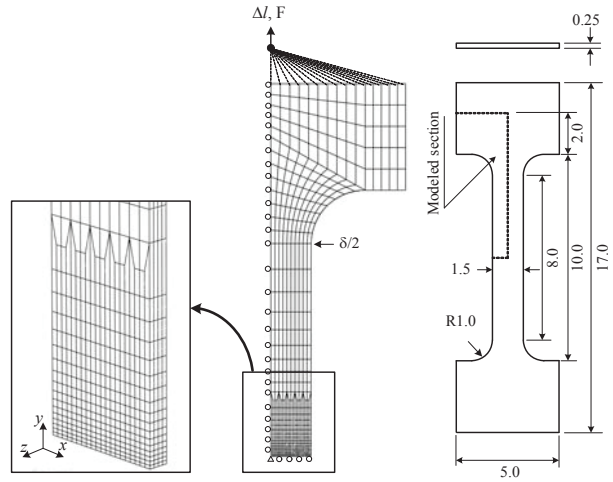

Fig. 2 Finite element model for simulation of tensile data

3. Finite Element Simulation

A procedure applied to determine full equivalent true stress-true strain curve including unstable plasticity regime in tensile deformation was the same as that described in the previous study [8]. The equivalent true stress-true strain relation to onset of necking was directly obtained from the experimental load (F)-displacement (δ) data using the following Eqs. (1) and (2):

$$\sigma_T = F/A_o(\delta/L_o+1) \quad (1)$$

$$\varepsilon_T = \ln(\delta/L_o+1) \quad (2)$$

where A_o is the initial cross-sectional area of specimen and L_o is the initial gage length.

The curve after onset of necking was determined by iterative FE simulations until the numerical calculation of the load and unstable deformation corresponded well with the experimental data. FE simulation was performed using a general-purpose finite element program, ABAQUS [10]. As shown in Fig. 2, the FE model used in the analysis is three-dimensional one-eighth model that consists of 20-node solid element with reduced integration (C3D20R in ABAQUS). Finer meshes were modeled near the center of the specimen where the strain gradient was expected to be large; at the center of the specimen twenty and four elements were layered in the width and thickness directions, respectively. The number of elements and element size were optimized based on the convergence test. Material and geometrical nonlinearities were considered in the analysis to properly simulate the necking of specimens: materials were modeled as isotropic elastic-plastic materials that obey the incremental plasticity theory. The nonlinear geometry option (NLGEOM) in the ABAQUS program was chosen to incorporate large geometry change. A geometrical imperfection in a form of localized reduced width and thickness of an amount 0.25% of their dimensions was embedded in the model to allow the initiation of necking. In spite that the material damage and bifurcation of specimen should be considered to accurately simulate the deformation beyond the onset of localized necking, these were not taken into account in the present model for simplicity.

In order to verify finite element model used in this study, the simulated and experimental load-displacement curves were compared in Fig. 3. In all cases, the predicted and measured loads and displacements at the onset of necking were almost identical. It was also possible to almost completely match the load-displacement curve with the experimental one for necking deformation up to the final failure. In particular, the simulated load agreed well with the experiment one even if σ_E- ε_E curves showed a pseudo-yield drop followed by continuous softening to final

failure. Therefore, it is believed that the FE model successfully simulates the load-displacement responses of tensile data including the early failure process such as the localized necking as well as global diffuse necking and that the deformation behavior and failure properties can be reliably calculated by FE simulation.

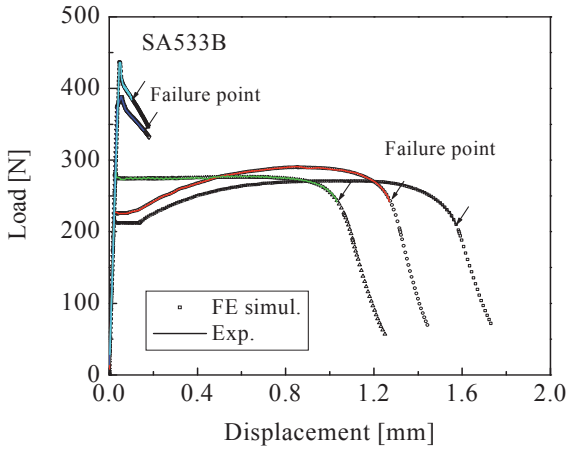

Fig. 3 Comparisons of load-displacement curves obtained from experiment and FE simulation for irradiated SA533B.

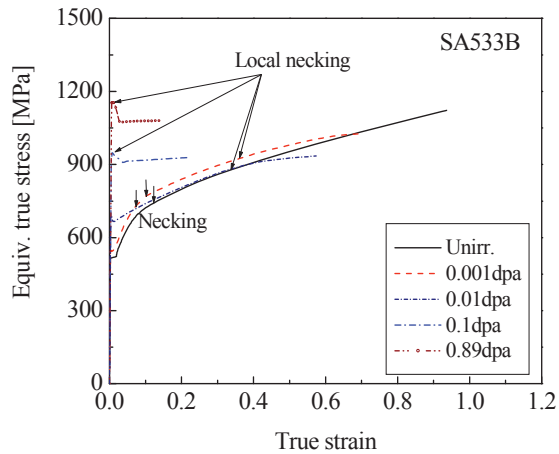

Fig. 4 Equivalent true stress-true strain curves of irradiated SA533B

4. Results and Discussion

4.1. Deformation behavior

Figure 4 presents full equivalent σ_T-ε_T curves including unstable necking deformation for SA533B steel irradiated to various doses, which were determined by the iterative FE simulations. At lower doses below 0.01dpa, the equivalent σ_T-ε_T curves are almost identical regardless of irradiation dose level, except that yield stress increases with increasing dose level. Above 0.1dpa, however, the equivalent σ_T-ε_T curves were clearly higher than those below 0.01dpa. Also, the curves at doses of 0.1 and 0.89dpa initially dropped and then increased with increasing true strain, even though the slope was lower than that at lower doses. This indicates that the strain hardening rate of irradiated SA533B is still positive regardless of irradiation dose level, even though the engineering stress-strain curves showed a continuous softening after yielding.

In order to examine influence of onset of necking on the equivalent σ_T-ε_T behavior for irradiated SA533B steel, the diffuse and localized necking points were indicted on the equivalent σ_T- ε_T curves shown in Fig. 4. The onset of localized necking was determined from the strain contour. It was indicated that onset of localized necking is evidenced by spreading maximum principal logarithmic stain contour along an oblique plane of specimen [8]. All specimens showed onset of localized necking before final failure. At doses below 0.001dpa, the localized necking was started after some amount of unstable plastic deformation by diffuse necking, and there was no slope change in the σ_T-ε_T curves at the onset of localized necking as well as diffuse necking. At dose of 0.01dpa, however, the slope of the σ_T-ε_T curve clearly reduced after onset of localized necking, and the reduced slope was similar to that at 0.1 and 0.89dpa. Above 0.1dpa where plastic instability occurred at yield, the onset of localized necking appeared at yield point without diffuse necking. Thus, the lower strain hardening rate at higher irradiation doses would be associated with early onset of localized necking rather than irradiation hardening mechanism.

Consequently, it is indicated that strain hardening rate in the equivalent σ_T- ε_T curve was still positive during the unstable necking deformation, even if a pseudo-yield drop followed by continuous softening appeared in σ_E-ε_E curves, and the strain hardening rate was sensitive to the necking mode transition rather than irradiation dose.

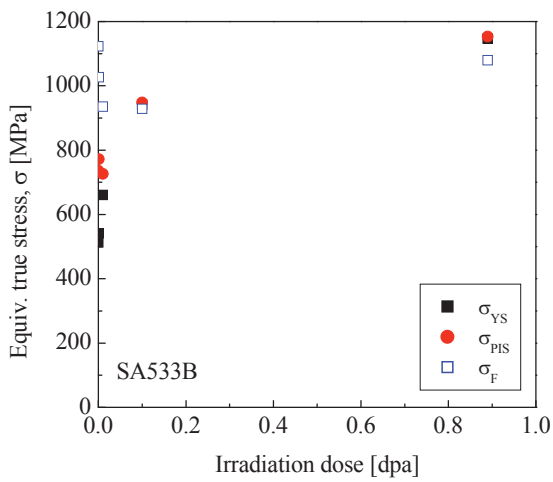

Fig. 5 Dose dependence of equivalent fracture stress for SA533B

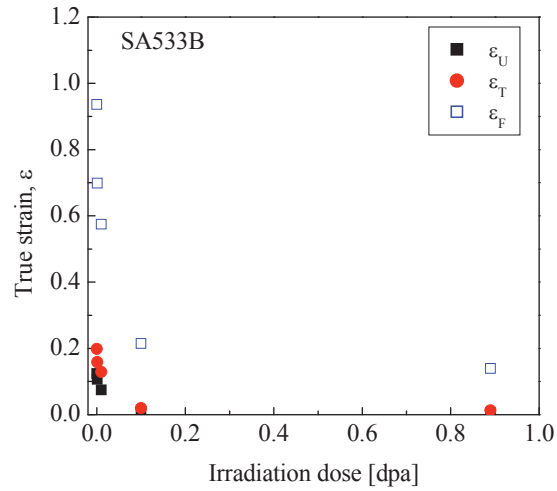

Fig. 6 Dose dependence of equivalent fracture strain for SA533B

4.2. Fracture properties

To investigate irradiation dose dependence of tensile fracture properties for SA533B steel, the equivalent fracture stress and fracture strain were obtained from equivalent true stress-true strain curves. As discussed above, all specimens showed onset of localized necking before final failure. Once the localized necking started at flat specimen, the strain was concentrated at the necking plane. Thus, the fracture strain was determined from the average value of maximum principal logarithmic strain over the localized necking plane at the displacement corresponding to final failure in the load-displacement curve. The equivalent fracture stress was determined as a stress value corresponding to the fracture strain on the equivalent σ_T- ε_T curve.

Figure 5 presents the equivalent fracture stresses for SA533B steel as a function of irradiation dose, together with the yield stress (σ_{YS}) and plastic instability stress (σ_{PIS}). The equivalent fracture stress decreased with increase in dose level up to 0.1dpa and slightly increased above dose level: the equivalent fracture stress at 0.89dpa was almost the same as that at 0dpa. It is seen that the equivalent fracture stress is less sensitive to irradiation dose compared to yield and plastic instability stresses, which considerably increased with increase in dose level up to 0.1dpa and then slightly increased above dose level; σ_{YS} at 0.89 dpa is about 2 times higher than that at 0dpa. Figure 6 presents the equivalent fracture strains as a function of irradiation dose, together with the uniform strain (ε_U) and total strain (ε_T). The equivalent fracture strain significantly decreased with increasing dose level up to 0.1dpa and then decreased at lower rate, but it was still high after irradiation exposure to 0.89dpa even if uniform ductility was almost zero.

Therefore, it is indicated that the fracture properties were sensitive to irradiation dose in the range of 0-0.1dpa and less sensitive above dose level. These dose dependences of tensile fracture stress and strain are related with the fact that density of irradiation induced defects increases with increasing dose and is saturated at dose around 0.05dpa.

5. Conclusions

This study evaluated true stress-strain curves of irradiated SA533B steel using finite element simulation and investigated the effects of irradiation dose on the deformation behavior and tensile fracture properties.

1) Localized necking occurred without diffuse necking when plastic instability occurred at yield.

2) Strain hardening rate in the equivalent true stress-strain curve was still positive during the unstable necking deformation, and it varied with necking mode change rather than with irradiation dose.

4) Equivalent fracture strain significantly decreased with increasing dose level up to 0.1dpa and then decreased at lower rate. But, it was still high after high dose irradiation exposure even if uniform ductility was almost zero.

Acknowledgements

This work has been supported by KESRI, which is funded by MKE (Ministry of Knowledge Economy).

References

[1] Dai Y, Egeland GW, Long B, Tensile properties of ferritic/martensitic steels irradiated in STIP-I. *J. Nucl. Mater*. 2008; **377**;115-21

[2] Pawel JE, Rowcliffe AF, Licas GE, Zinkle SJ, Irradiation performance of stainless steels for ITER application, *J. Nucl. Mater*. 1996;**239**;126-31.

[3] Farrell K, Byun TS, Tensile properties of candidate SNS target container materials after proton and neutron irradiation in the LANSCE accelerator, *J. Nucl. Mater*. 2001;**296**;129-38

[4] Farrell K, Byun TS, Hashimoto N, Deformation mode maps for tensile deformation of neutron-irradiated structural alloys. *J. Nucl. Mater.* 2004;**335**; 471-86

[5] Byun TS, Farrell K, Plastic instability in polycrystalline metals after low temperature irradiation. *Acta Mater*. 2004;52;1597-608

[6] Byun TS, Dose dependence of true stress parameters in irradiated bcc, fcc, and hcp metals. *J. Nucl. Mater*. 2007;**361**;239-47

[7] Byun TS, Farrell K, Lee EH, Hunn JD, Mansur LK, Strain hardening and plastic instability properties of austenitic stainless steels after proton and neutron irradiation. *J. Nucl. Mater*. 2001;**298**;269-79

[8] Kim JW, Byun TS., Analysis of tensile deformation and failure in austenitic stainless steels: Part II-Irradiation dose dependence. *J. Nucl. Mater.* 2010; **396**;10-9.

[9] Ling Y, Uniaxial true stress-strain after necking. *AMP J. Tech*. 1996;**5l**;37-48.

[10] Hibbitt, Karlson, and Sorensen Inc., 2010. ABAQUS Ver. 6.9 User's Manual.